

Supporting Information

Unexpected wavelength dependency of the photocatalytic CO₂ reduction performance of the well-known (bpy)Re(CO)₃Cl

Philipp Lang,^{†a} Robin Giereth,^{†b} Stefanie Tschierlei^{*b} and Matthias Schwalbe^{*a}

TOC graphic:

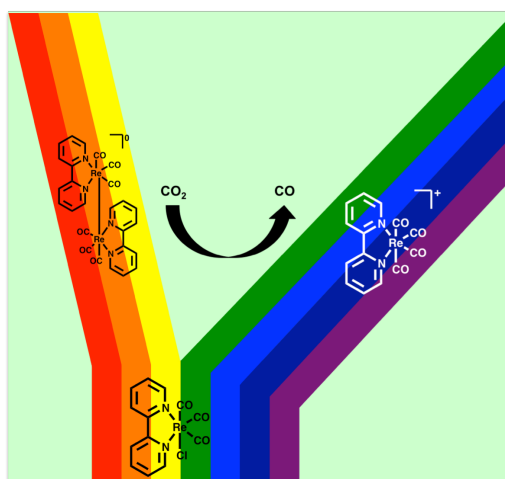


Table of Content:

1. General Methods	2
2. Synthesis and Characterization	4
2.1. Synthesis of (bpy)Re(CO) ₃ Cl	4
2.2. Synthesis of [(bpy)Re(CO) ₄]OTf	4
2.3. Synthesis of [Re ⁰ (bpy)(CO) ₃] ₂	4
3. Photocatalysis	5
3.1. Influence of the light source and the sacrificial electron donor on the photocatalytic activity	5
3.2. Time dependent photocatalysis	5
3.3. Time dependent CO evolution of [(bpy)Re(CO) ₄]OTf and [Re ⁰ (bpy)(CO) ₃] ₂	6
4. UV/vis studies	7
5. DFT calculations and IR spectroscopy	8
6. Cyclovoltammetry	13
7. Spectroelectrochemistry	14
8. Emission characteristics of excitation source	15

1. General Methods

Column chromatography was performed with silica gel purchased from VWR or Acros (Silica Gel 60, 230–400 μm mesh). All solvents and starting materials were obtained from Sigma-Aldrich. If necessary, solvents were dried employing a MBraun solvent purification system. Starting materials were used without further purification. DMF for photolysis experiments was obtained dry in sealed flasks from Merck and triethylamine for photocatalytic reactions was refluxed with KOH, filtered, and dried with CaH_2 . TEOA was dried with a molecular sieve (4 \AA) and stored under argon. 1,3-Dimethyl-2-phenyl-2,3-dihydro-1H-benzo[d]imidazole (BIH) was synthesized according to literature.¹

¹H NMR spectra were recorded at ambient temperature on either a Bruker DPX-300 or AV-400 spectrometer. All spectra were referenced to tetramethylsilane (TMS) or deuterated chloroform (CDCl_3) as an internal standard (measured values for δ are given in ppm and for J in Hz).

UV/vis absorption spectroscopic measurements were done on DCM solutions or directly from catalytic mixtures (DMF/TEA(5%)) using a Cary 100 UV/vis-NIR spectrometer from Varian employing the software Cary WinUV. SUPRASIL Quartz cells from Hellma Analytics with a 10 mm path length were used.

Irradiation experiments were performed either in DMF with 5% TEA as sacrificial electron donor or in DMF/TEOA 5:1 with 2000eq of BIH with 5×10^{-5} M catalyst concentration. Fresh solutions were prepared before each experiment in Schlenk flasks with 5 mL of solution and 20 mL of headspace, and they were bubbled with CO_2 for 20 min to remove argon. Photolysis was performed with a 200 W high-pressure-mercury-vapor lamp using a water filter to absorb IR radiation and different long-wave pass cut-off filters to absorb wavelengths below the given values. Filters ($\lambda > 305$, $\lambda > 325$, $\lambda > 350$, $\lambda > 375$, $\lambda > 400$, $\lambda > 450$ and $\lambda > 500$ nm) were purchased from LOT-QuantumDesign GmbH and had a sharp edge of $\Delta = \pm 3$ nm (transmission spectra see Fig S11). CO and H_2 evolved were determined by gas chromatography (Shimadzu GC-17A with thermal conductivity detector and Resteks ShinCarbon packed column ST 80/100 (2 m, 1/8 in. o.d., 2 mm i.d.) and quantified using a calibration curve. Measurements were done by manual injection of gas phase samples (250 μL) at least in duplicate. CO or H_2 dissolved in the solvent was not considered, thus the TON of CO is only related to the amount detected in the gas phase above the solution. To estimate the amount of CO that was produced by other sources, like solvent decomposition, photolysis experiments were done without the catalyst under the same conditions and all turnover numbers of CO were corrected by these values. In these blank experiments, no CO was detected using $\lambda > 350$ nm cut-off filter and higher, while TON_{CO} values obtained with the $\lambda > 305$ nm filter were corrected by a value of 0.8 after 24 hours of illumination.

Light intensity measurements were performed using a ASMETEC TM-209 LED Light Meter.

Cyclic voltammetry of $(\text{bpy})\text{Re}(\text{CO})_3\text{Cl}$ (1 mM) was carried out in DMF or acetonitrile with 0.1 M Bu_4NPF_6 as the supporting electrolyte. The measurements were performed with an Autolab potentiostat PGSTAT204 from Metrohm using a three-electrode configuration. As working electrode, a glassy carbon disc with a 3 mm diameter stick was used. The counter electrode was a Pt electrode. As reference electrode, a non-aqueous Ag/Ag^+ electrode (0.01 M AgNO_3 in acetonitrile) was utilized with the ferrocene/ferrocenium (Fc/Fc^+) couple as reference, added to the solution after each experiment. Thus, all reported potentials are *versus* the Fc/Fc^+ couple. All scan rates are 0.1 V/s unless otherwise noted. The solutions were purged with argon prior to every measurement.

1 a) E. Hasegawa, T. Seida, N. Chiba, T. Takahashi, H. Ikeda, *J. Org. Chem.* 2005, **70**, 9632; b) Y. Tamaki, K. Koike, T. Morimoto and O. Ishitani, *J. Catal.*, 2013, **304**, 22.

UV/vis spectroelectrochemistry at room temperature was conducted with a commercial “honeycomb” thin-layer SEC cell from Pine Research Instrumentation, employing a screen-printed platinum working and counter electrode and a silver/silver chloride pseudo-reference electrode.² The constant cell potential during the SEC measurements were applied with an Autolab potentiostat PGSTAT204 from Metrohm. The UV/vis measurements were performed in a SPECORD s600 photodiode array spectrophotometer with an overall integration time of 250 ms (5 accumulations with 50 ms integration time). The solutions were thoroughly purged with argon prior to every measurement. For measurements under CO₂ atmosphere, the solutions were saturated with CO₂ gas. The concentration of analyte and supporting electrolyte was the same as in the cyclic voltammetry measurements.

DFT calculations. Simulations at the density functional theory (DFT) level were performed using the ORCA program package (Version 4.0.1.2).³ All calculations used triple zeta valence plus polarization functions (def2-TZVP) basis sets.⁴ In order to speed up the calculations, the resolution of identity approximation (RI) with a suitable optimized auxiliary basis set was used.^{4,5} Excited state calculations on dimeric species (**8**, **9**) were performed with the def2-SVP basis set, due to computational costs. Geometry optimizations were carried out in redundant internal coordinates. Solvation effects were accounted for by the conductor-like polarizable continuum model, CPCM, with an appropriate dielectric constant and refractive index of DMF. For geometry optimizations of the electronic ground state the BP86 and B3-LYP exchange-correlation functional were used.⁶ The SCF cycles in geometry optimizations and TD-DFT calculations were iterated up to the point where the energy changed by less than 1E-9 atomic units (less than 1E-14 atomic units for BP86 calculations). To ensure converged ground-state geometries, a convergence criterion for the maximum change in energy of at least 1E-8 atomic units (1E-10 a. u. for B3-LYP optimizations) and a maximum gradient of at least 1E-4 with a maximal RMS gradient of 1E-5 was chosen. All stationary points on the potential energy surface of the S₀ state were verified by calculations of the energy second derivatives with respect to nuclear coordinates. Excited state calculations were carried out with the B3-LYP functional, starting from ground state structures optimized with the B3-LYP functional. To account for dispersion effects, the DFTD3 V3.1 correction (D3) by S. Grimme including the Becke-Johnson (BJ) damping is used throughout all calculations.⁷ For the calculation of excited states at the time-dependent density functional theory level, the Tamm-Dancoff approximation (tda-TD-DFT) was used. Visualizations of electron density difference maps were carried out with VMD.⁸

2 V.V. Pavlishchuk and A.W. Addison, *Inorg. Chim. Acta*, 2000, **298**, 97.

3 a) F. Neese, *WIREs Comput. Mol. Sci.*, 2017, **8** b) F. Neese, *Interdiscip. Rev. Comput. Mol. Sci.*, 2012, **2**, 73.

4 F. Weigend and R. Ahlrichs, *Phys. Chem. Chem. Phys.*, 2005, **7**, 3297.

5 K. Eichkorn, O. Treutler, H. Öhm, M. Häser and R. Ahlrichs, *Chem. Phys. Lett.*, 1995, **242**, 652.

6 O. Treutler and R. Ahlrichs, *J. Chem. Phys.*, 1995, **102**, 346.

7 a) S. Grimme, J. Antony, S. Ehrlich and H. Krieg, *J. Chem. Phys.*, 2010, **132**, 154104. b) S. Grimme, S. Ehrlich and L. Goerigk, *J. Comput. Chem.*, 2011, **32**, 1456.

8 W. Humphrey, A. Dalke and K. Schulten, "VMD - Visual Molecular Dynamics", *J. Molec. Graphics*, 1996, **14**, 33-38; <http://www.ks.uiuc.edu/Research/vmd/>

2. Synthesis and Characterization

2.1. Synthesis of (bpy)Re(CO)₃Cl

(bpy)Re(CO)₃Cl was synthesized according to a literature method.⁹ Under argon atmosphere Re(CO)₅Cl (0.302 g, 0.83 mmol) and 2,2'-bipyridine (0.130 g, 0.83 mmol) were dissolved in 50 mL toluene and the reaction mixture was stirred at reflux for 3 h. Within the first 5 min of applying heat the solution began to turn yellow, and the intensity of color increased with time during reflux. The solvent was subsequently removed under reduced pressure, and the product was purified by column chromatography. Impurities were first eluted with DCM, and the product was finally eluted with DCM:MeOH = 97:3. The target complex was isolated as yellow solid with an overall yield of 92% and good agreement of analytical data to the literature.

2.2. Synthesis of [(bpy)Re(CO)₄]OTf

[(bpy)Re(CO)₄]OTf was synthesized according to a literature method.¹⁰ Re(CO)₅Cl (0.40 g, 1.1 mmol) was dissolved in 80 mL DCM in a round bottom flask. AgOTf (0.30 g, 1.2 mmol) dissolved in 20 mL DCM was added to the flask. The reaction mixture was left stirring at room temperature in the dark under argon for 21 hours. AgCl precipitate was filtered off and washed with 30 mL DCM. 0.19 g (1.2 mmol) 2,2'-bipyridine was added to the filtrate and the reaction was allowed to stir for 8 hours in the dark under inert atmosphere. The reaction mixture was concentrated in vacuo to 20 mL, and 100 mL of hexanes was added to precipitate a yellow solid that was subsequently removed by filtration and dried. The target complex was isolated in satisfying purity with an overall yield of 55% and good agreement of analytical data to the literature.

2.3. Synthesis of [Re⁰(bpy)(CO)₃]₂

(bpy)Re(CO)₃Cl (0.100 g, 0.217 mmol) was added to 20 mL THF under inert atmosphere. The solution was cooled to -35 °C and 1.1 eq. (0.032 g, 0.238 mmol) of KC₈ was added to the solution and allowed to warm to room temperature. After an hour, the solution was filtered through a plug of silica gel, and the column was washed with an additional 20 mL of THF. The solvent was removed in vacuo to afford a dark green powder with a yield of 54% and with good agreement of analytical data to the literature.¹¹

9 L.A. Worl, R. Duesing, P.Y. Chen, L. Dellaciana and T.J. Meyer, *J. Chem. Soc., Dalton Trans.* 1991, **0**, 849.

10 K.A. Grice, N.X. Gu, D. Sampson and C.P. Kubiak, *Dalton Trans.*, 2013, **42**, 8498.

11 E.E. Benson and C.P. Kubiak, *Chem. Commun.*, 2012, **48**, 7374.

3. Photocatalysis

3.1. Influence of the light source and the sacrificial electron donor on the photocatalytic activity

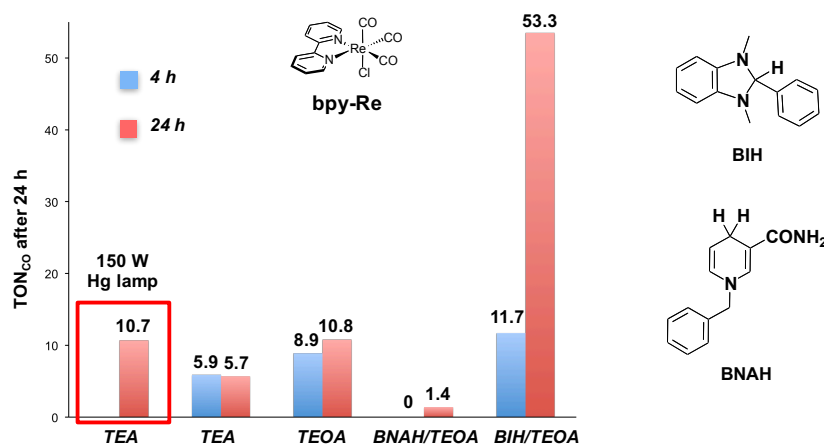


Figure S1 - Summary of catalytic results using $5 \cdot 10^{-5}$ M (bpy)Re(CO)₃Cl (**1**), a $\lambda > 450$ nm cutoff filter and different electron donors in DMF under 1 atm CO₂ (TEA: 5 % or TEOA: 17 % (with 2000 eq. of BNAH or BIH)). Note that a 200 W Xe Arc-lamp has been used in these experiments except for the first one.

These findings are in accordance with the lower oxidation potential of BIH compared to TEA (0.33 V vs. 0.69 V, respectively, versus SCE)¹² and hence a facilitated reductive quenching mechanism.

3.2. Time dependent photocatalysis

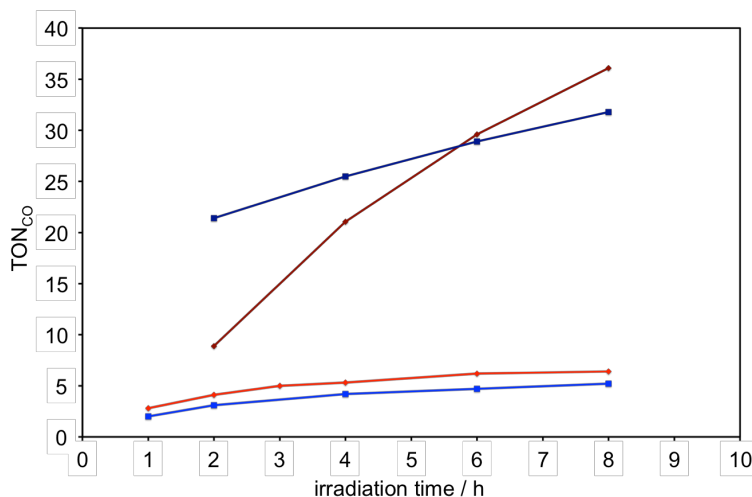


Figure S2 - Time dependent CO evolution for (bpy)Re(CO)₃Cl in DMF/TEA(5%) ($\lambda > 450$ (red), $\lambda > 305$ nm (blue)) and in DMF with TEOA(17%)/BIH(2000eq) ($\lambda > 450$ (dark red), $\lambda > 305$ nm (dark blue)) in the first 8 hours of illumination.

Independent of the electron donor used, the appearance of the overall CO evolution curves is very similar using illumination light > 305 nm. However, substantially faster decomposition is observed using TEA as electron donor compared to BIH when light > 450 nm is used. Similar results have been obtained before and can be related to poisoning degradation products that are formed due to TEA decomposition.¹³

12 Y. Pellegrin and F. Odobel, *C. R. Chimie*, 2017, **20**, 283.

13 a) P.J. DeLaive, T.K. Foreman, C. Giannotti and D.G. Whitten, *J. Am. Chem. Soc.*, 1980, **102**, 5627; b) Y. Tamaki and O. Ishitani, *ACS Catal.*, 2017, **7**, 3394.

3.3 Time dependent CO evolution of $[(bpy)Re(CO)_4]OTf$ and $[Re^0(bpy)(CO)_3]_2$

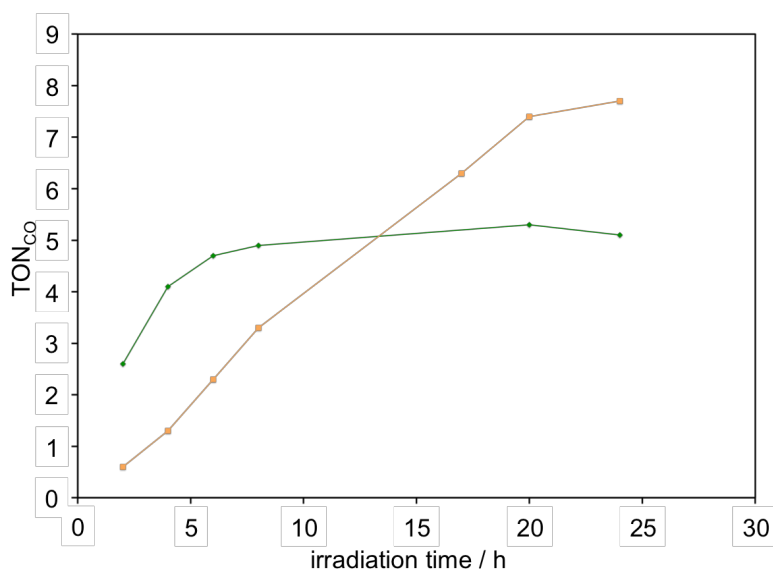


Figure S3 - Time dependent CO evolution for $[(bpy)Re(CO)_4]OTf$ (**6**, orange) and $[Re^0(bpy)(CO)_3]_2$ (**8**, green) under irradiation with $\lambda > 450$ nm in DMF/TEA(5%)

Tab. S1 - TON values for $[(bpy)Re(CO)_4]OTf$ (**6**) after 24 h of irradiation in DMF with 5% TEA as sacrificial electron donor and results of blank experiments without either light, electron donor or CO₂

Sacrificial electron donor	Illumination	TON _{CO}
TEA	$\lambda > 450$ nm	7.7
TEA	(dark)	0.6
-	$\lambda > 450$ nm	0
TEA without CO ₂	$\lambda > 450$ nm	0

(Small amounts of CO are released in the dark indicating that slow substitution of CO takes place, probably by a DMF molecule. Note that ligand exchange has been observed before, albeit not in acetonitrile for **1**, and is facilitated upon reduction.¹⁰)

Tab. S2 - TON values of $[Re^0(bpy)(CO)_3]_2$ (**8**) after 24 h of irradiation in DMF with 5% TEA as sacrificial electron donor and results of blank experiments without either light, electron donor or CO₂

Sacrificial electron donor	Illumination	TON _{CO}
TEA	$\lambda > 450$ nm	5.3
TEA	(dark)	0.3
-	$\lambda > 450$ nm	0.2
TEA without CO ₂	$\lambda > 450$ nm	0

4. UV/vis studies

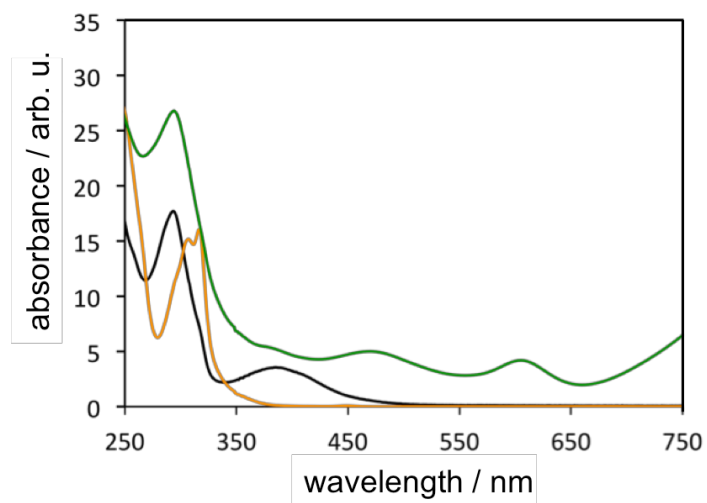
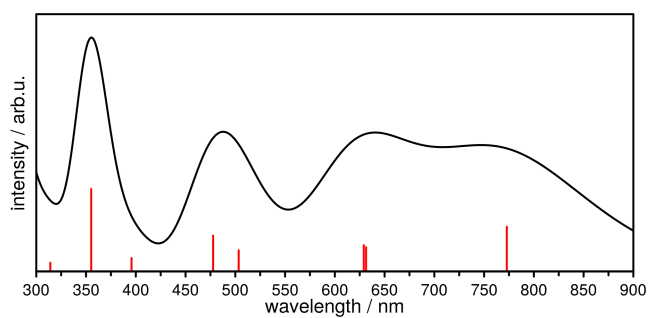
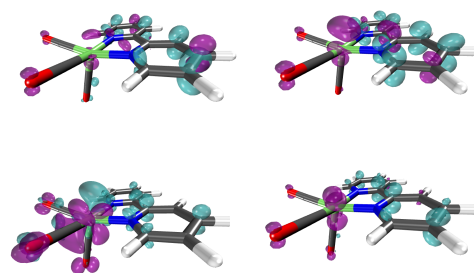


Figure S4 - UV/vis absorption spectra of $(\text{bpy})\text{Re}(\text{CO})_3\text{Cl}$ (**1**, black), $[(\text{bpy})\text{Re}(\text{CO})_4]\text{OTf}$ (**6**, orange) and $[\text{Re}^0(\text{bpy})(\text{CO})_3]_2$ (**8**, green) in DCM.

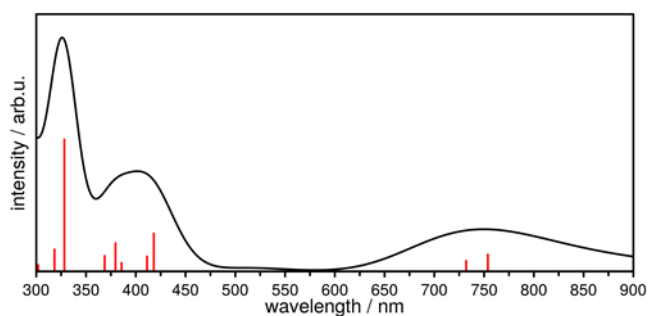
5. DFT calculations and IR spectroscopy



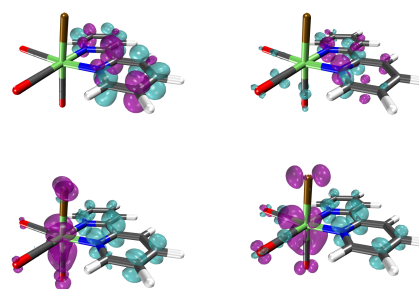
2



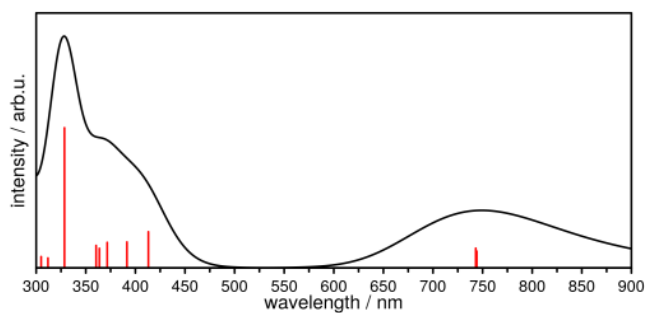
top: states 1, 3. bottom: states 7, 13



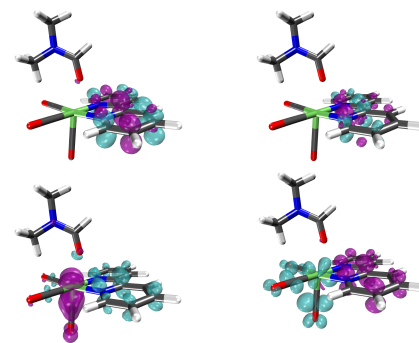
2Cl



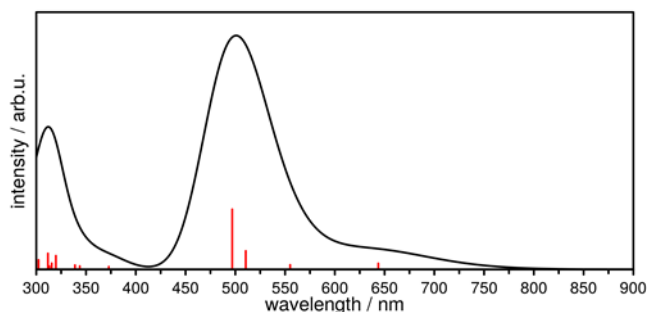
top: states 2, 6. bottom: states 7, 9



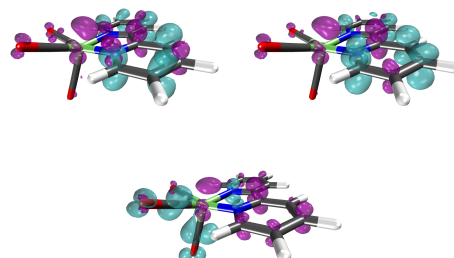
2DMF



top: states 2, 7. bottom: states 9, 11



3



top: states 1, 3. bottom: state 4

Figure S5 – TDDFT (B3LYP-D3(BJ)/def2-TZVP) calculation of **2**, **2Cl**, **2DMF** and **3**. Left: result from the convolution of the transitions (red sticks) with a Gaussian function. Right: differential density plots for the most dominant transitions (cyan corresponds to a positive isovalue between the single-electron matrices of the ground and excited state; purple corresponds to a negative isovalue, and hence, a decline in electron density). Compare also with excitation characteristics listed in Table S3.

Due to the nature of the electron localization in the one electron reduced species there is a dynamic equilibrium between **2Cl** and **2S** (S being a solvent molecule).¹⁶ Only the second reduction process brings about the rapid cleavage of the Re-halide bond.¹⁴ These assignments and findings are also in accordance to UV/vis spectroelectrochemical measurements performed on an anthracene-bridged bimetallic Re₂ complex.¹⁵

The calculated UV/vis spectra of the one electron reduced species (**2**, **2Cl** and **2DMF**) are in accordance with the literature with bands at 500 nm and weak broad components around 750 nm.^{16,17}

14 F. Paolucci, M. Marcaccio, C. Paradisi, S. Roffia, C. Bignozzi and C. Amatore, *J. Phys. Chem. B*, 1998, **102**, 4759.

15 W. Yang, S.S. Roy, W.C. Pitts, R.L. Nelson, F.R. Fronczek and J.W. Jurss, *Inorg. Chem.*, 2018, **57**, 9564.

16 Y. Hayashi, S. Kita, B.S. Brunshwig and E. Fujita, *J. Am. Chem. Soc.*, 2003, **125**, 11976.

17 H. Takeda, K. Koike, H Inoue and O. Ishitani, *J. Am. Chem. Soc.*, 2008, **130**, 2023.

Tab. S3 - Calculated excitation energies and transitions of **2**, **2Cl**, **2DMF**, **3** and **8** at TD-DFT level (B3LYP-D3(BJ)/def2-TZVP) with CPCM (DMF) solvation model. Only oscillator strengths > 0.01 and corresponding orbital contributions with $|\text{coeff.}|^2 * 100 > 0.19$ are listed.

2

State #	Excitation energy		Oscillator strength	Dominant contributions			Transitions
	cm ⁻¹	nm		occ. orb.	virt. Orb.	$ \text{coeff.} ^2 * 100$	
1	12940.2	772.8	0.07096474	HOMO	LUMO	0.837052	$d_{Re}, \pi_{bpy}^*, n_{CO} \rightarrow d_{Re}, \pi_{bpy}^*$
2	15836.6	631.4	0.03840383	HOMO	LUMO+2	0.846281	$d_{Re}, \pi_{bpy}^*, n_{CO} \rightarrow \pi_{bpy}^*, \pi_{CO,ax}^*$
3	15896.2	629.1	0.041687	HOMO	LUMO+1	0.926091	$d_{Re}, \pi_{bpy}^*, n_{CO} \rightarrow \pi_{bpy}^*$
6	19866.7	503.4	0.03365882	HOMO-2	HOMO	0.647436	$d_{Re}, n_{CO,eq.} \rightarrow d_{Re}, \pi_{bpy}^*, n_{CO}$
				HOMO-3	HOMO	0.239040	$d_{Re}, n_{CO} \rightarrow d_{Re}, \pi_{bpy}^*, n_{CO}$
7	20934.5	477.7	0.05688389	HOMO-3	HOMO	0.667822	$d_{Re}, n_{CO} \rightarrow d_{Re}, \pi_{bpy}^*, n_{CO}$
8	25274.1	395.7	0.0212382	HOMO-4	HOMO	0.541677	$\pi_{bpy}^* \rightarrow d_{Re}, \pi_{bpy}^*, n_{CO}$
				HOMO-1	LUMO	0.278130	$d_{Re}, n_{CO,ax.} \rightarrow d_{Re}, \pi_{bpy}^*$
13	28151.1	355.2	0.13084239	HOMO	LUMO+5	0.550809	$d_{Re}, \pi_{bpy}^*, n_{CO} \rightarrow \pi_{bpy}^*$
23	31836.3	314.1	0.01380967	HOMO	LUMO+8	0.814179	$d_{Re}, \pi_{bpy}^*, n_{CO} \rightarrow d_{Re}, \pi_{CO}^*$

2Cl

State #	Excitation energy		Oscillator strength	Dominant contributions			Transitions
	cm ⁻¹	nm		occ. orb.	virt. Orb.	$ \text{coeff.} ^2 * 100$	
2	13265.8	753.8	0.02658157	HOMO	LUMO+1	0.941010	$\pi_{bpy}^* \rightarrow \pi_{bpy}^*$
6	23917.7	418.1	0.05943599	HOMO	LUMO+3	0.956828	$\pi_{bpy}^* \rightarrow \pi_{CO}^*$
				HOMO	LUMO+5	0.694474	$\pi_{bpy}^* \rightarrow \pi_{bpy}^*$
7	24312.8	411.3	0.02345738	HOMO-1	HOMO	0.883174	$d_{Re}, n_{CO} \rightarrow \pi_{bpy}^*$
9	26343.8	379.6	0.04430888	HOMO-2	HOMO	0.825047	$d_{Re}, n_{CO} \rightarrow \pi_{bpy}^*$
10	25928	385.7	0.01352267	HOMO	LUMO+7	0.856554	$\pi_{bpy}^* \rightarrow d_{Re}, \pi_{CO}^*$
13	27118.9	368.7	0.02448892	HOMO	LUMO+9	0.777082	$\pi_{bpy}^* \rightarrow d_{Re}, \pi_{CO}^*$
14	30465.2	328.2	0.20664366	HOMO-3	HOMO	0.447804	$d_{Re}, n_{CO,ax.} \rightarrow \pi_{bpy}^*$
16	31418.2	318.3	0.0345748	HOMO-1	LUMO+3	0.259382	$d_{Re}, n_{CO} \rightarrow \pi_{CO}^*$

2DMF

State #	Excitation energy		Oscillator strength	Dominant contributions			Transitions
	cm ⁻¹	nm		occ. orb.	virt. Orb.	$ \text{coeff.} ^2 * 100$	
2	13456.4	743.1	0.02920746	HOMO	LUMO+1	0.925089	$\pi_{bpy}^* \rightarrow \pi_{bpy}^*$
7	24209.8	413.1	0.05362376	HOMO	LUMO+3	0.922383	$\pi_{bpy}^* \rightarrow \pi_{CO}^*$
				HOMO	LUMO+6	0.690577	$\pi_{bpy}^* \rightarrow \pi_{bpy}^*$
9	25541.4	391.5	0.03843315	HOMO-1	HOMO	0.811675	$d_{Re}, n_{CO} \rightarrow \pi_{bpy}^*$
10	27493.9	363.7	0.02898091	HOMO-2	HOMO	0.707828	$d_{Re}, n_{CO}, n_{O,DMF} \rightarrow \pi_{bpy}^*$
11	26912.4	371.6	0.03781082	HOMO	LUMO+9	0.645318	$\pi_{bpy}^* \rightarrow d_{Re}, \pi_{CO}^*$
14	27745.9	360.4	0.03325908	HOMO	LUMO+10	0.744804	$\pi_{bpy}^* \rightarrow d_{Re}, \pi_{CO}^*$
15	30440.8	328.5	0.20795287	HOMO-3	HOMO	0.455110	$d_{Re}, n_{CO,eq.} \rightarrow \pi_{bpy}^*$
				HOMO	LUMO+10	0.224961	$\pi_{bpy}^* \rightarrow d_{Re}, \pi_{CO}^*$
17	32066.6	311.9	0.01468839	HOMO-1	LUMO	0.251166	$d_{Re}, n_{CO} \rightarrow \pi_{bpy}^*, \pi_{CO,eq.}^*$

Tab. S3, continued - Calculated excitation energies and transitions of **2**, **2Cl**, **2DMF**, **3** and **8** at TD-DFT level (B3LYP-D3(BJ)/def2-TZVP) with CPCM (DMF) solvation model. Only oscillator strengths > 0.01 and corresponding orbital contributions with |coeff.|²*100 > 0.19 are listed.

3

State #	Excitation energy		Oscillator strength	Dominant contributions			Transitions
	cm ⁻¹	nm		occ. orb.	virt. Orb.	coeff. ² *100	
1	15534.2	643.7	0.0284149	HOMO	LUMO	0.332719	$d_{Re}, \pi_{CO}^* \rightarrow d_{Re}, \pi_{bpy}^*, \pi_{CO}^*$
2	18014.6	555.1	0.02159054	HOMO	LUMO+1	0.638369	$d_{Re}, \pi_{CO}^* \rightarrow \pi_{bpy}^*, \pi_{CO}^*$
3	19588.6	510.5	0.08669827	HOMO	LUMO+3	0.893536	$d_{Re}, \pi_{CO}^* \rightarrow \pi_{CO}^*$
				HOMO	LUMO+2	0.865918	$d_{Re}, \pi_{CO}^* \rightarrow \pi_{bpy}^*$
4	20125.2	496.9	0.28125067	HOMO	LUMO	0.516111	$d_{Re}, \pi_{CO}^* \rightarrow d_{Re}, \pi_{bpy}^*, \pi_{CO}^*$
				HOMO	LUMO+1	0.312156	$d_{Re}, \pi_{CO}^* \rightarrow \pi_{bpy}^*, \pi_{CO}^*$
6	26818.2	372.9	0.01300181	HOMO-1	LUMO	0.429180	$d_{Re}, n_{CO} \rightarrow d_{Re}, \pi_{bpy}^*, \pi_{CO}^*$
8	29092.3	343.7	0.01582977	HOMO	LUMO+4	0.470372	$d_{Re}, \pi_{CO}^* \rightarrow \pi_{CO}^*$
				HOMO	LUMO+5	0.802384	$d_{Re}, \pi_{CO}^* \rightarrow d_{Re}, \pi_{CO}^*$
9	29506.5	338.9	0.02027421	HOMO-3	LUMO	0.288760	$d_{Re}, n_{CO} \rightarrow d_{Re}, \pi_{bpy}^*, \pi_{CO}^*$
				HOMO-2	LUMO	0.450501	$d_{Re}, n_{CO} \rightarrow d_{Re}, \pi_{bpy}^*, \pi_{CO}^*$
11	31276.5	319.7	0.06423813	HOMO	LUMO+6	0.618527	$d_{Re}, \pi_{CO}^* \rightarrow \pi_{bpy}^*$
13	31694.1	315.5	0.02898447	HOMO	LUMO+8	0.662012	$d_{Re}, \pi_{CO}^* \rightarrow d_{Re}, \pi_{bpy}^*$
				HOMO-1	LUMO+1	0.567253	$d_{Re}, n_{CO} \rightarrow \pi_{bpy}^*, \pi_{CO}^*$
14	32077.3	311.7	0.07503733	HOMO-1	LUMO+2	0.686471	$d_{Re}, n_{CO} \rightarrow \pi_{bpy}^*$

8

State #	Excitation energy		Oscillator strength	Dominant contributions			Transitions
	cm ⁻¹	nm		occ. orb.	virt. Orb.	coeff. ² *100	
1	13862.3	721.4	0.11972441	HOMO	LUMO	0.946621	$\sigma_{Re-Re} \rightarrow \pi_{bpy}^*$
2	18156.4	550.8	0.09025311	HOMO	LUMO+1	0.830790	$\sigma_{Re-Re} \rightarrow \sigma_{Re-Re}^*, \pi_{bpy}^*$
4	21493.9	465.2	0.08303108	HOMO	LUMO+2	0.954681	$\sigma_{Re-Re} \rightarrow \pi_{bpy-1}^*$
8	23835.8	419.5	0.01959262	HOMO	LUMO+3	0.944263	$\sigma_{Re-Re} \rightarrow \pi_{bpy-2}^*$
9	22794.8	438.7	0.08112397	HOMO	LUMO+6	0.770876	$\sigma_{Re-Re} \rightarrow \pi_{CO}^*$
				HOMO-1	LUMO	0.495257	$d_{Re} \rightarrow \pi_{bpy}^*$

bpy-1: stacked pyridine rings; bpy-2: non-stacked pyridine rings

Vibrational frequency calculations allow us to compare/verify the compounds. as the C≡O modes are very sensitive towards the electronic nature of the complex. The calculated frequencies of intermediates such as **1**, **3**, **6** or **8**. are in reasonable accordance with experimental data.^{9,18}

Tab. S4 – Comparison of experimentally determined and calculated IR frequencies of the C≡O modes.

complex		solvent	ν _{C≡O}				reference	
Re ^I (bpy)(CO) ₃ Cl	1	DMF	1893	1914	2019		16c	
	1	calc.	1850	1862	1983			
	1	THF	1895	1917	2019		19	
Re ⁰ (bpy)(CO) ₃ Cl	2	DMF	1862	1880	1994		16c	
	2	calc.	1827	1833	1946			
	2DMF	calc.	1835	1835	1962			
	2Cl	calc.	1817	1826	1951			
[Re(bpy)(CO) ₃ Cl] ¹⁻	3	calc.	1764	1769	1881			
	3	THF	1866	1880	1998		17	
[Re ⁰ (bpy)(CO) ₃] ₂	8	THF	1862	1886	1952	1990	10	
	8	calc.	1814	1824	1834	1843	1920	1945
	8	THF	1863	1886	1952	1990		17

18 a) G. Stor, F. Hartl, J. Van Outersterp and D. Stufkens, *Organometallics*, 1995, **14**, 1115; b) J. Smieja and C. Kubiak, *Inorg. Chem.*, 2010, **49**, 9283; c) F. Johnsin, M. George, F. Hartl and J. Turner, *Organometallics*, 1996, **15**, 3374; d) A. Klein, C. Vogler and W. Keim, *Organometallics*, 1996, **15**, 236.
19 E. Fujita and T. Muckermann, *Inorg. Chem.*, 2004, **43**, 7673.

6. Cyclovoltammetry

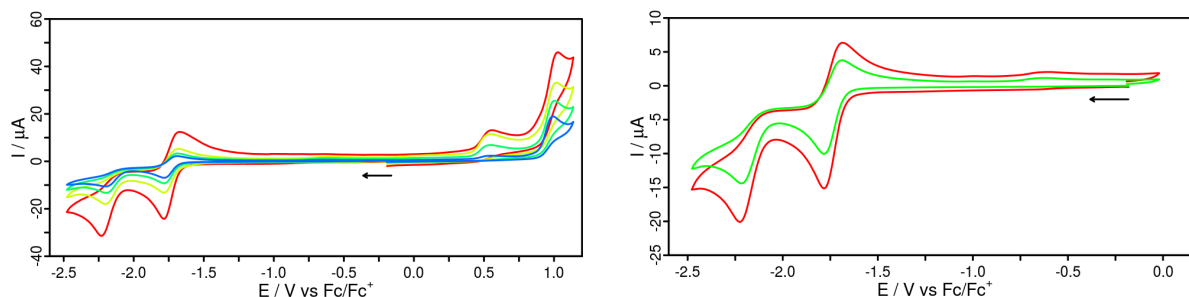


Figure S7 - Cyclic voltammogram of (bpy)Re(CO)₃Cl **1** in DMF with 0.1 M Bu₄NPF₆ as supporting electrolyte at different scan rates and referenced vs. the ferrocene/ferrocenium couple. The first reversible reduction event occurs at a half-step potential of $E_{1/2} = -1.75$ V. The second irreversible reduction has an anodic peak at -2.24 V which is in accordance to the literature.²⁰

Left: Oxidation and reduction events are displayed at scan rates of 25 mV/s (blue), 50 mV/s (green), 100 mV/s (yellow) and 250 mV/s (red).
 Right: Display of the two reduction processes at the scan rates of 50 mV/s (green) and 100 mV/s (red).

Tab. S5 – Reduction potentials of **1** and **8**, whereby the reduction potential of **8** is very close to that of **1**.²⁰

Complex	Potential [V]
1	$E_{1/2} = -1.75$ V
1^a	$E_{1/2} = -1.76$ V
[Re(CO) ₃ (bpy)(ACN)] ⁺	$E_{1/2} = -2.17$ V
8^a	$E_{1/2} = -1.94$ V $E_{II}^P = -2.24$ V ^b

a from ref. 20

b homolytic bond cleavage **8** → 2x **3**

7. Spectroelectrochemistry

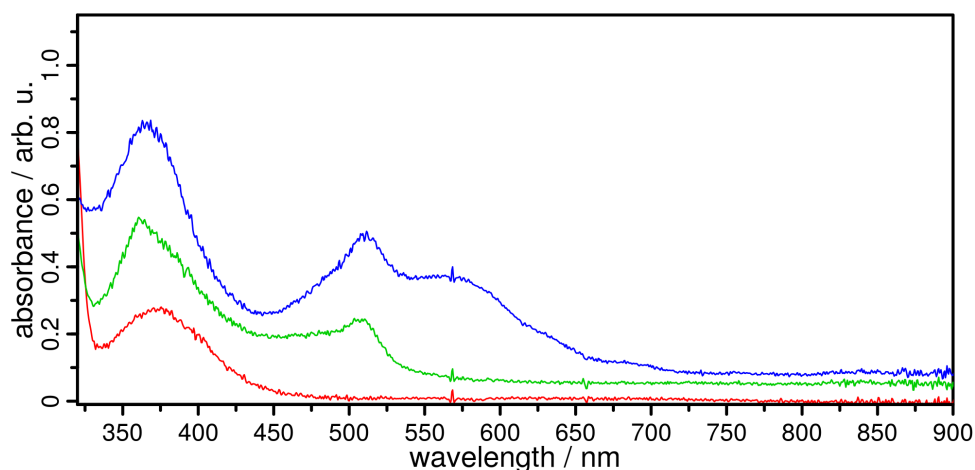


Figure S8 - UV/vis spectrum of 0.5 mM **1** in DMF with applied reduction potentials at -1.62 V (green) and -2.02 V (blue) vs. Fc/Fc⁺. For comparison, the spectrum of the unreduced complex **1** (red) is given.

The UV/vis spectrum of **1** under deaerated conditions obtained at an applied potential of -1.62 V (vs. Fc/Fc⁺, a bit anodic than the redox potential of $E^{1/2} = -1.75$ V, Figure S7) displays the growth of an absorption band at 508 nm as well as an increase and slight blueshift of the MLCT band from 375 nm to 362 nm. This is characteristic for the generation of the one-electron reduced rhenium species **2** (**2Cl** or **2DMF**). Applying a slightly higher potential of -2.02 V (vs. Fc/Fc⁺, Figure S7) a new absorption band at 574 nm appears, which can be assigned to the generation of **3**. The bands of **2** (**2Cl** or **2DMF**) are still obvious, because the reduction process is not sufficient and the one-electron reduced rhenium species is still present in the solution. In principle, the applied potential in our experiment should not be sufficient to produce **3**, because the respective reduction potential is much more cathodic. Thus, it seems that a dimerization to **8** occurs and this intermediate is reduced more easily to **3** (see the main text).

8. Emission characteristics of excitation source

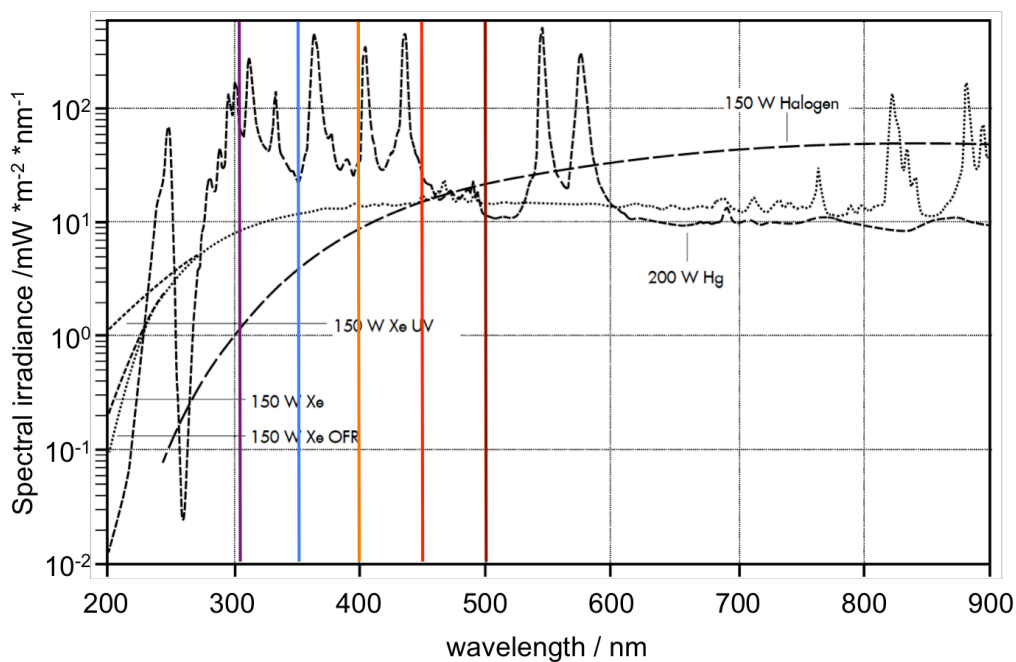


Figure S9 – Characteristic emission spectrum of the used 200 W Hg-vapor lamp. Provided with courtesy by LOT-Quantum Design GmbH (color code is similar to the cut off filters in Fig. S10).

In Table S6 we list the measured light intensities when applying the different cut-off filters. It is obvious that the intensities only change slightly and thus, this difference cannot account for the different photocatalytic performance that we observe.

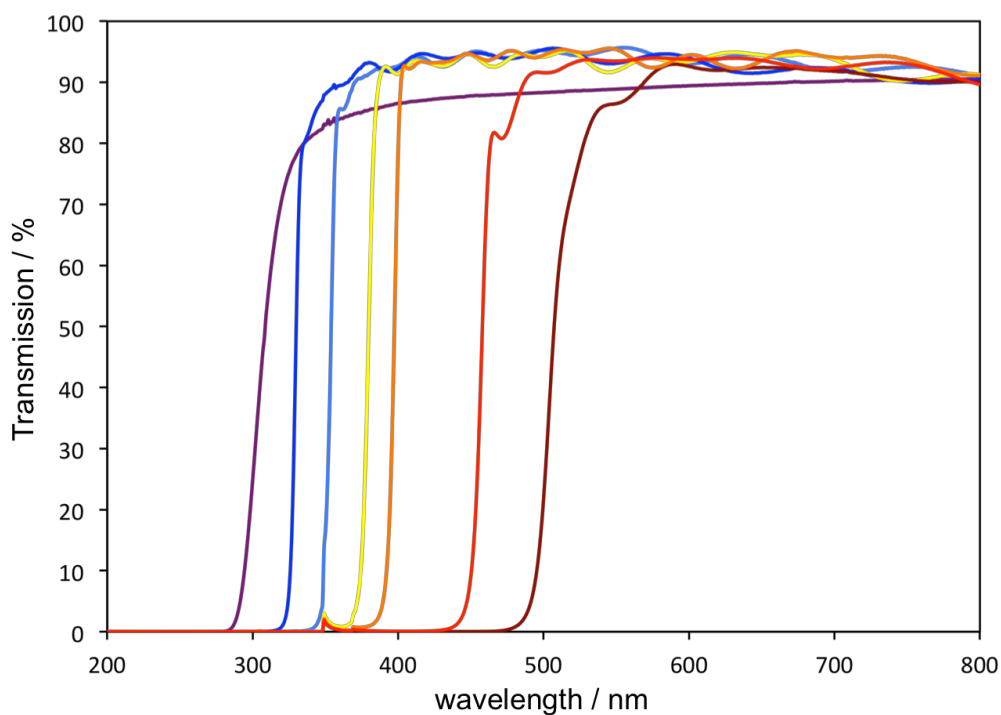


Figure S10 – Characteristic transmission spectra of the used cut-off filters: $\lambda > 305$ (purple), $\lambda > 325$ (dark blue), $\lambda > 350$ (blue), $\lambda > 375$ (yellow), $\lambda > 400$ (orange), $\lambda > 450$ (red), $\lambda > 500$ (dark red).

Tab. S6 – Measured light intensities of the Hg-vapour lamp by application of the different cut-off filters with a ASMETEC TM-209 LED Light Meter. (To avoid detector saturation a neutral density filter (1.00 ND) was used additionally; please note that the light meter only detects in the spectral region of 375 – 800 nm.)

Cut-off Filter	Intensity / Lx
$\lambda > 375 \text{ nm}$	69200 (+/- 500)
$\lambda > 400 \text{ nm}$	69200 (+/- 500)
$\lambda > 450 \text{ nm}$	65000 (+/- 500)
$\lambda > 500 \text{ nm}$	62100 (+/- 500)